PhotoniX

RESEARCH Open Access

Frequency selective fingerprint sensor: the Terahertz unity platform for broadband chiral enantiomers multiplexed signals and narrowband molecular AIT enhancement

Jiaming Lyu[1], Shengyuan Shen[1], Lin Chen[1,2*], Yiming Zhu[1*] and Songlin Zhuang[1]

*Correspondence:
linchen@usst.edu.cn;
ymzhu@usst.edu.cn

[1] Terahertz Technology Innovation Research Institute, Terahertz Spectrum and Imaging Technology Cooperative, Innovation Center Shanghai Key Lab of Modern Optical System University of Shanghai for Science and Technology, Shanghai 200093, China
[2] Shanghai Institute of Intelligent Science and Technology, Tongji University, Shanghai 200092, China

Abstract

Chiral enantiomers have different pharmacological and pharmacokinetic characteristics. It is important to strictly detect chiral component for avoiding being harmful to the human body due to side effects. Terahertz (THz) trace fingerprint detection is essential because the molecular vibrations of various biological substances such as chiral enantiomers are located in THz range. Recent reported enhanced trace fingerprint technologies have some drawbacks. For instance, multiplexing technology suffered from narrow operation range and limitation by frequency resolution of commercial THz time domain spectroscopy; Absorption induced transparency (AIT) identification for narrowband molecular oscillations suffered from random resonance frequency drift due to fabrication error. In this paper, we proposed frequency-selective fingerprint sensor (FSFS), which can experimentally achieve enhanced trace fingerprint detection by both broadband multiplexing technology and robust AIT identification. Such FSFS is based on polarization independent reconfiguration metasurfaces array. Broadband absorption lines of trace-amount chiral carnitine were boosted with absorption enhancement factors of about 7.3 times based on frequency-selective multiplexing at 0.95–2.0 THz. Enhanced trace narrowband α-lactose fingerprint sensing can be observed at several array structures with absorption enhancement factors of about 7 times based on AIT, exhibiting good robustness. The flexibility and versatility of proposed FSFS has potential applications for boosting trace chiral enantiomer detection as well as diversity of molecular fingerprints identification by both multiplexing and AIT.

Keywords: Chiral enantiomer, Frequency-selective fingerprint sensor, Multiplexing, Absorption induced transparency, Fingerprints identification

Introduction

Chiral enantiomers have the same structural groups, but the rotation direction is different [1]. The enantiomers can be divided into D-type and L-type. The chemical properties of D-type and L-type chiral enantiomers are significant different in pharmacological activity [2] and toxicity [3]. Misjudgment of D-type or L-type chiral enantiomers may be harmful to the human body. Therefore, it is of great significance to identify chiral components. There are some existing detection methods of chiral enantiomers. For instance, mass spectrometry can only identify molecules with different molecular weight and functional groups. It cannot distinguish chiral enantiomers with same molecular weight [4]. Chemical methods, such as chiral solvation reagent method [5], are not able to do trace detection. For the Raman spectroscopy, the chemical formula of the whole molecule is deduced mainly by testing the characteristic peaks of the molecular bonds and functional groups [6]. However, for chiral molecules, their chemical bonds and functional groups are completely consistent and cannot be identified [7].

Terahertz (THz) wave is located in the frequency range of 0.1–10 THz electromagnetic spectrum, which has the advantages of noninvasive and nonionizing properties [8]. THz spectroscopy has attracted wide attention due to its non-contact, label-free, broadband detection, and energy matching with intermolecular interactions, such as translational and rotational energy of a molecule [9–11]. The rotation directions of chiral molecules and the corresponding vibration rotation amplitudes or frequencies are different. The physical mechanism and recognition process of chiral enantiomers could be analyzed based on their fingerprint frequencies and corresponding amplitudes [7, 12]. However, THz spectroscopic measurements of chiral enantiomers usually need to press the powdered sample into a pellet, which is not suitable for trace sensing [7]. To overcome this difficulty, Chang et al. [13] used vibrational circular dichroism of chiral metasurface to identify optically active substances with different molar absorptivity, which were used for the qualitative analysis of chiral enantiomers. However, due to the large number of low energy conformations of some flexible molecules, the vibrational circular dichroism method has low reliability [14]. Therefore, there is still an urgent need for quantitative detection of trace chiral enantiomers in biomedicine.

There are several THz metamaterial sensors for trace detection with different applications. For instance, the toroidal resonance are used to realize refractive index (RI) sensing of highly absorptive analytes [15]. Then I-shape metasurface design was proposed to enhance sensitivity by optimizing the value of the mode volume of the metamaterial resonantly confined fields [16]. A microfluidic metasensor was also demonstrated to realize size selective trapping and sensing of microparticles. The maximum blue shift of 10 GHz is achieved for 15% particle trapping rate [17]. In addition, bound state in the continuum mode was also excited and illustrated to achieve metamaterial sensing with high sensitivity by coating Ge film [18]. More recently, A topological sensor consists of a topological waveguide critically coupled with an ultra-high Q topological cavity was demonstrated with high figure of merit sensing performance [19]. Moreover, the electromagnetic induced transparency cloak senor was demonstrated, which is invisible to the incident THz wave [20]. From these work we can see that THz metasensors were widely applied in various fields [21]. However, this detection method ignores the specific identification of terahertz fingerprint spectrum of analytes. For quantitative trace detection

in biomedicine, an antibody modified terahertz metamaterial biosensor was successfully realized to detect the concentration of carcinoem bryonic antigen by exciting the induction-capacitance resonance [22]. Furthermore, a terahertz metasurface immunosensor coupled with gold nanoparticles was proposed by exciting electric dipole resonance, which shows good biocompatibility and high specific surface area for biomarkers [23]. In addition, the metasurface with strong magnetic resonances was designed as an aptamer modified biosensor to specifically detect the human epidermal growth factor receptor 2 with the limit-of-detection of 0.1 ng/mL [24]. However, this detection methods are more complex due to antibody modified process.

Up to now, there are two mechanisms that can achieve THz trace molecular fingerprint sensing: absorption induced transparency (AIT) [25, 26] and multiplexing technology [27–30]. The most intriguing characteristic of AIT is that the transmission peak, in the combined metasurface device with analyte system, appears at the spectral position where the bare analyte presents resonant absorption. This effect has been demonstrated in THz region using arrangement metallic grating [25] and split-ring resonators [26]. However, additional shifting of the metasurface resonance due to the nondispersive component (real permittivity) of the analyte and fabrication error make the metasurface resonance difficult to match the resonance frequency of the analyte covered system. More recently, multiplexing array has been used to trace chiral enantiomers/isomer molecular fingerprint sensing due to strong light–matter interaction between a series of narrowband resonant peaks of metasurfaces with broadband mode resonance of chiral enantiomers/isomers [30]. Here, the absorption of the trace chiral enantiomers/isomers can be obviously enhanced in broadband spectrum by changing the incident angle and/or unit cell geometry. Despite the widely used all-dielectric metasurfaces in mid-infrared fingerprint metasensing [27, 28], the THz all-dielectric metasurfaces may suffer from nonnegligible surface undulation which requires complicated and dedicated conformal coating interface engineering. In addition, the enhancement spectrum range is generally narrowband. Moreover, few experimental results were reported for multiplexing THz fingerprint sensing by all-dielectric metasurfaces because the ultra-narrow linewidth of resonance was hardly observed by commercial terahertz time-domain spectroscopy (THz-TDS). Finally, the ultra-narrow resonance is hard to excite AIT, which enables the enhanced trace fingerprint observation much easier under the conditions of larger linewidth of metasurface resonance than that of analyte [31, 32]. Consideration of two enhanced trace molecular fingerprint sensing methods, it is of great importance to design reconfigurable metasurfaces with acceptable linewidth to achieve intriguing characteristics of both AIT and multiplexing for elevating the different type of THz molecular fingerprint detection of trace analytes.

In this paper, frequency selective fingerprint sensor (FSFS) was designed in application of enhanced THz fingerprint trace sensing. The scheme is based on symmetric crossed-slot resonators with identical width of the horizontal and vertical slots which shows polarization independence. In addition, a high transmittance and enhanced Q factor can be simultaneously achieved by optimized cross slot. For broadband absorption lines such as chiral carnitine (D-carnitine and L-carnitine), 36 resonance peaks with acceptable linewidth by scanning length of slots were used to realize broadband trace THz absorption enhancement. Here frequency-selective feature can be easily realized by

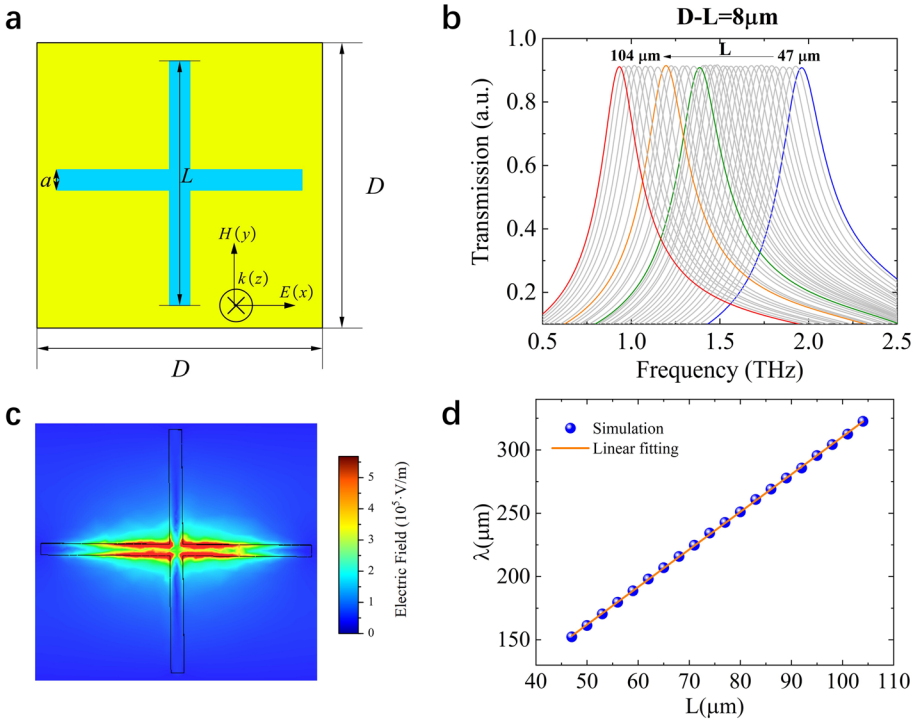

Fig. 1 **a** Crossed-slot structure in a unit cell lattice. **b** Numerically simulated FSFS transmission spectra for different values of crossed-slot length L, maintain a = 5 μm, and D-L = 8 μm. **c** Electric field distribution of L = 47 μm at resonance frequency in the unit cell. **d** The central resonance wavelength with respect to the crossed-slot length L

simply tuning length of slots. Absorption enhancement factors of about 7.3 times can be achieved in an ultra-wide terahertz band for 10 μm thick chiral carnitine film. For narrow absorption line such as α-lactose monohydrate, the AIT was observed due to larger linewidth of plasmonic metasurface resonance than that of α-lactose monohydrate. The observation of AIT in pixels group shows excellent robustness. The FSFS platform gives a diverse way to facilitate the metasensing of the THz trace fingerprint for both broadband chiral enantiomers absorption lines by multiplexing and narrowband analyses spectral width by AIT.

FSFS platform design

The metallic aperture-coupled resonators that comprised of cross slot elements were used to realize the polarization independence FSFS because of their excellent reconfigurable behavior. To improve transmission efficiency and maintain high Q factor, we proposed symmetric crossed-slot resonators with identical width of the horizontal and vertical slots. The geometry structure and parameters of the designed cross slot unit cell are shown in Fig. 1a. There are three major geometric parameters, namely, the cross-slot unit length (L), the slit width (a) and the periodicity (D). If we choose a = 5 μm, and maintain D-L = 8 μm, the center frequency of the metasurfaces mainly depends on L. Figure 1b presents the simulated transmission spectra of the metasurface with the y-polarized illumination. The input THz wave propagates through the metasurface in normal incidence. The simulations have been carried out by three-dimensional full wave

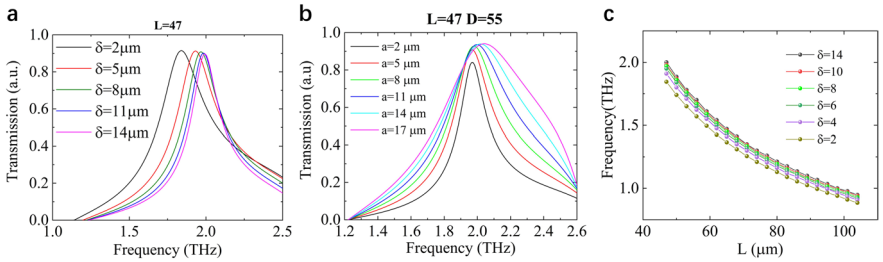

Fig. 2 The transmission response with (**a**) various δ ((D-L)/2), (**b**) slot width a, (**c**) the transmission response with various δ by scanning L

simulations based on a Finite Integration Technique in the frequency domain (CST Microwave Studio). The permittivity of the fused quartz substrate was 3.84 with a loss tangent tan δ = 0.001, and the electrical conductivity of gold is 4.561×10^7 S/m [33, 34]. Simulated transmission spectra of a 6 × 6 FSFS with a cross-shaped unit length variation from L = 47 μm to L = 104 μm show sharp resonance peaks with almost unity transmission intensity covering the spectral range from 0.9 to 2.0 THz (Fig. 1b). Figure 1c shows a simulated two-dimensional profile of electric field distribution in the unit cell at the resonance frequency f = 1.93 THz (L = 47 μm) as incident light is with y-polarization. The electric field is localized around the middle part of the horizontal slot. Similarly, for the incident light with x-polarization, the electric field is localized along the vertical slot. Such enhancement of the local electric near field intensity confined to the resonator surface is ideal for the sensitive detection of analyte molecular vibrations. The polarization-independent characteristic of proposed cross slot metasurfaces is also given in supplementary materials of Section 1.

The unit cell of cross slot metasurface structures can be equivalent to a resonant circuit based on the transmission line model in supplementary materials of Section 2. The central frequency of the circuit depends on the inductance (L), the resistor (R), and the capacitance (C) [35]. The central wavelength of this cross-structured metasurface can be roughly determined by the following empirical formula according to the approach of Anderson and Marcuvitz in supplementary materials of Section 2:

$$\lambda(\mu\mathrm{m}) = 2.971L(\mu\mathrm{m}) + 13.424 \tag{1}$$

The resonance peaks show excellent linear tunability of the resonance positions with correlation coefficient R^2 = 0.99987 (Fig. 1d) [36].

To further assess the influence of geometrical parameters on the transmission response, we investigate the influence of periodicity (D) on the resonance frequency as L is 47 μm, as shown in Fig. 2a. With the increase of D from 49 μm to 55 μm, the frequency shows blue shift and Q factor becomes larger. With further increase of D, the frequency and Q factor show very little change. So, D = 55 μm and δ = 8 μm are optimal values for achieving high Q design. Moreover, the transmission response with various slot width at fixed slot length (L) and periodicity (D) demonstrates that the larger the slot width is, the smaller the Q is (Fig. 2b). With the consideration of both fabrication errors and performance, we chose a as 5 μm. Finally, the transmission response with fixed slot width (a = 5 μm) and various δ (δ = (D-L)/2) was plotted in Fig. 2c. By

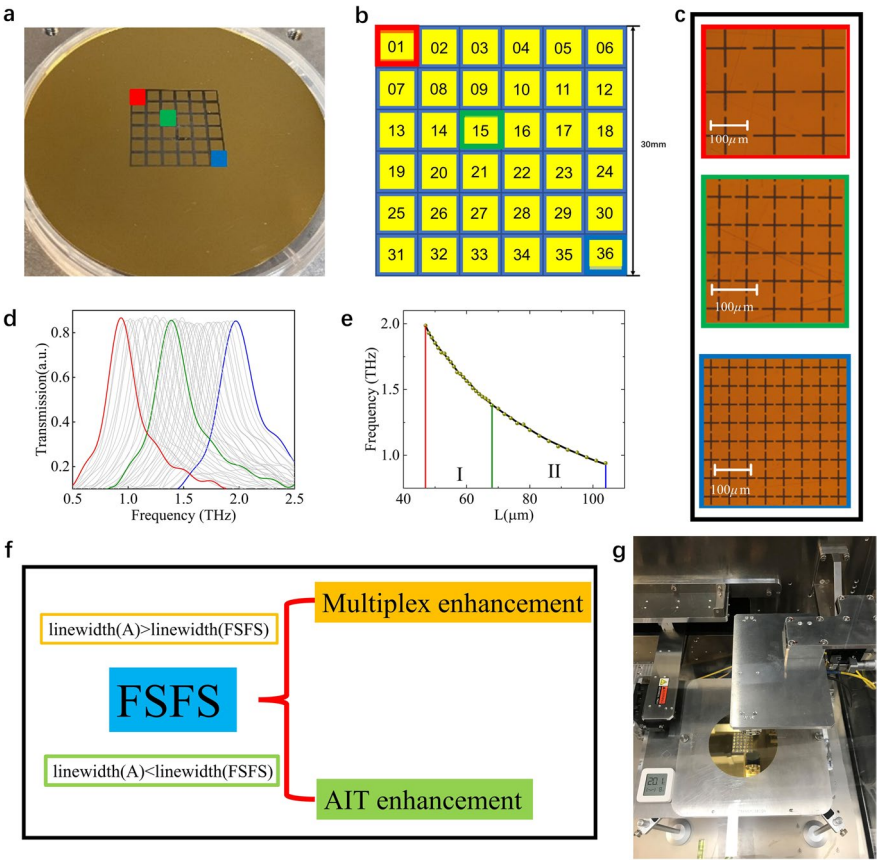

Fig. 3 **a** Optical images of the fabricated FSFS. **b** 36-pixel location (P1-P36 corresponds to L from 104 μm to 47 μm. **c** Microscope images of cross slot pixels for L = 104 μm (P1, red), 68 μm (P15, green) and 47 μm (P36, blue). **d** Normalized experimental transmission spectra of FSFS. **e** Experimental resonance frequencies vs L, inset: The interval L between 47 μm to 68 μm is denser in order to guarantee the interval of resonance frequency in each pixel less than 0.05 THz. **f** Operation principle of FSFS. **g** Trace detection scenario of FSFS

scanning L, the frequency shows slight red shift with different δ. In conclusion, we chose a = 5 μm, δ = 8 μm for detecting and differentiating the absorption signature.

The FSFS was fabricated by conventional photolithography and metallization processing. The fused quartz (Corning Corporation) is compatible with a wide temperature range from − 50 to + 150 °C, and material parameters is stable over this temperature range. A 150-nm-thick Au film was deposited on a fused quartz substrate. Figure 3a shows the optical image of FSFS, which has 6*6 pixels array. The 36 pixel positions (P1 ~ P36) arranged according to L (104 μm ~ 47 μm), as shown in Fig. 3b. The microscope photograph of the pixels which exhibits in the FSFS (Fig. 3c), corresponding to L = 47 μm (P36), 68 μm (P15), and 104 μm (P1). Each pixel in the pixel array is 3 mm*3 mm. Take L = 62 μm for example, the wave forms transmitted through the cross slot unit cell and the corresponding transmission spectrum of the transmitted pulses are given in supplementary materials of Section 3. The experimental results of all 36 pixels (Fig. 3d) show that the transmission curves and the resonance frequencies are in good agreement with the simulation (Fig. 1b). Figure 3e plotted experimental resonance frequencies with respect to L, which also fit well with simulations. The central frequencies deviation of pixel number between simulation and experiment are

given in supplementary materials of Section 4. The discrepancy between the simulated and measured resonances might be due to differences in the cross-slot structure parameters arising from random fabrication errors. Figure 3f shows operation principle of FSFS, which has the ability to excite both AIT enhancement due to the coherent coupling of a broadband mode of the metasurface to a narrowband mode resonance of analyte, and multiplex enhancement due to interaction of narrowband metasurface with broadband absorption line of analyte. This versatile platform offers many possibilities for trace THz molecular fingerprint sensing. We demonstrate two illustrative examples: the AIT enhancement for α-lactose, and the multiplex enhancement for chiral carnitine. We show that both of these functions can be used in commercial THz time-domain spectroscopy system, as illustrated in Fig. 3g (for instance, Advantest TAS 7400 in this work with frequency resolution of 7.6 GHz).

Enhanced AIT by FSFS

Here, we investigated AIT in the coherent coupling between a narrow band absorption resonance of α-lactose monohydrate and the resonances by FSFS. The Lorentz dispersion model as the dielectric function of analyze is adopted to illustrate its characteristic absorption spectra [37]

$$\varepsilon(\omega) = \varepsilon_\infty + \sum_{j=1}^{m} \frac{f_j \omega_{0j}^2}{\left(\omega_{0j}^2 - \omega^2\right) + i\gamma_j \omega} \tag{2}$$

where m is the number of oscillators with resonance frequency ω_{oj}; ω_p is the plasma frequency; f_j is the oscillator strength; ε_∞ is the dielectric coefficient with an infinite frequency, and γ is the damping constant, i.e. the full width half maximum (FWHM). The real and imaginary parts of the refractive index are defined as $n + i\kappa = \varepsilon^{1/2}$.

The frequencies of α-lactose corresponding to the absorption peaks exhibits a spectrally narrowband, strong resonance at a frequency of 1.37 THz in 0.9 – 2.0 THz range (Fig. 4a) [38]. For studying the coupling between FSFS and analyses, we investigated the interaction process between FSFS and 1 μm thick layer of α-lactose. We observed a symmetric splitting near 1.37 THz with the 65 μm slot length, which indicate coherent coupling between the cross slot resonance and the lactose resonance (Fig. 4b). The interactions between the localized surface plasmons and the molecular absorption are also called AIT (the equivalent AIT model is established in supplementary materials of Section 5). We note that such clear symmetric splitting can be found at metasurface resonance frequency 1.444 THz (L = 65 μm), which is larger than 1.37 THz. Such mismatch is due to the nondispersive component of the α-lactose permittivity, corresponding to ε_∞. In addition, compared to the dip with the 65 μm slot length (Fig. 4b), the AIT profile with 67 μm slot length in Fig. 4c show slight asymmetry. It can also be found that when the pixel resonances are less than 1.444 THz (L > 65 μm), the left peak of AIT is higher than the right peak. On the contrary, the left peak of AIT is lower than the right peak.

In experiment, we coated cross slot metasurface pixels with 1 μm thick layer of α-lactose by diluting α-lactose powder in a saturated aqueous solution and deposited it on top of the pixels. The absorption spectra of 1 μm thick α-lactose were measured, as shown in Fig. 4d and e (red line, multiply by 40 times). The spectral position and features

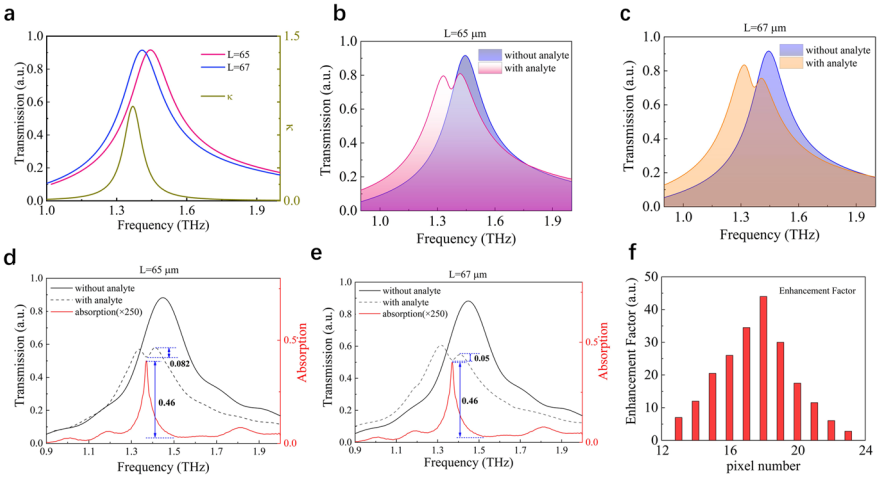

Fig. 4 Spectrally selective fingerprinting of analyte from FSFS. **a** The transmission spectra of the FSFS for pixel P18 (L = 65 μm) and P16 (L = 67 μm) and the imaginary parts of the complex dielectric function (Absorption spectra) of lactose. **b**, **c** Normalized transmissions in the presence and absence of analyte molecules with L = 65 μm (**b**) and 67 μm (**c**). Measured absorption spectrum of α-lactose (red) and observation of AIT in a FSFS/α-lactose system (dash line) with (**d**) L = 65 μm (**e**) L = 67 μm. **f** Enhancement factor (define as the extinction ratio of the transmission dip of AIT divide by analyte absorption peak) as a function of pixel number, which confirms the robustness of AIT enhancement by FSFS

of the α-lactose signal presented here are close to the simulation in Fig. 4a. The amplitude transmission spectra of FSFS of L = 65 μm (P18) and 67 μm (P16) with (dash line) and without (solid line) 1 μm-thick α-lactose were measured, which is also shown in Fig. 4d and e, respectively. The result shows that a clear change of resonance shape was found due to AIT excitation. There is a vibrational signal located at 1.38 THz, which is close to conventional sensing results (1.37 THz). The transmission profiles of AIT by the dash curves in Fig. 4d and e agree well with the simulations in Fig. 4b and c. The enhancement factor is defined as the ratio of smaller AIT dip difference and conventional absorption amplitude (marked in Fig. 4d and e). Figure 4f plotted the enhancement factor with respect to pixel number. The maximum enhancement factor can achieve 7 times at P18 (L = 65 μm) and the AIT effect can be observed in a broad pixel range from P13 to P23. Our FSFS can capture narrow absorption line of analyte regardless of thickness uncertainty of analyte and the robustness of AIT can be enhanced by covering large pixels range.

Enhanced chiral substances multiplex signals by FSFS

We also use this FSFS to the identification of trace chiral substances by scanning and boosting the absorption spectra. The THz absorption spectra of carnitine (D-carnitine and L-carnitine) show two broadband absorption lines [7]. We can also use Eq. 2 with the frequencies corresponding to the absorption peaks are 1.39 and 1.72 THz, respectively. In simulation results as shown in Fig. 5a and b, a 10 μm carnitine layer covering FSFS causes a pronounced modulation of the individual pixel transmission spectra due to the coupling between the molecular vibrations and the enhanced electric fields around the cross-slot resonators. This transmission modulation is correlated with the D-carnitine and L-carnitine molecular vibrations [7]. The envelopes of the pixel absorption spectra

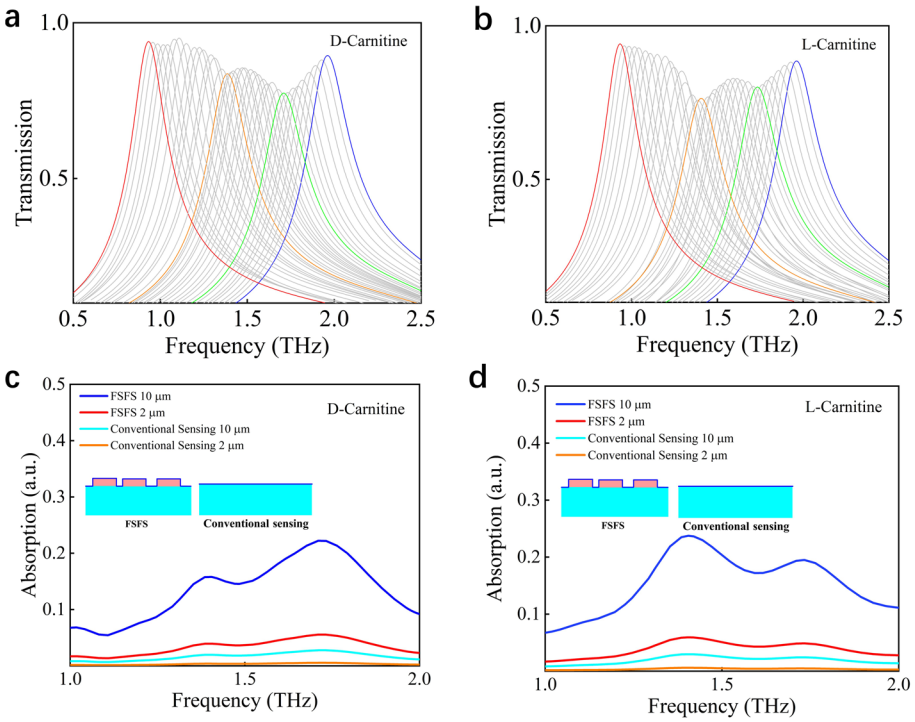

Fig. 5 Upper: Simulated normalized transmissions of (**a**) D-carnitine and (**b**) L-carnitine by FSFS multiplexing; bottom: Simulated absorbance envelopes of (**c**) D-carnitine and (**d**) L-carnitine with various thicknesses by conventional sensing and FSFS

for 1 μm and 10 μm thick chiral carnitine are illustrated in Fig. 5c and d, respectively. For comparison, the conventional THz absorption spectra of D-carnitine and L-carnitine are also plotted in Fig. 5c and d by fitting the Eq. 2 according to Ref. [7]. The absorption peak positions of D-carnitine and L-carnitine are basically the same, and D-carnitine and L-carnitine show two absorption peak frequencies of 1.39 THz and 1.72 THz except that absorption of D-Carnitine is lower than that of L-Carnitine at 1.39 THz, and absorption of D-Carnitine is higher than that of L-Carnitine at 1.72 THz. If the thickness of chiral carnitine is thin, the error of qualitative analysis increases, and the absorption peak position cannot be found in conventional sensing. The FSFS reproduces the broadband carnitine absorption signature. At 1.39 THz and 1.72 THz, the absorption amplitudes boosted about 8.1 times for 10 μm thick analyses and 9.8 times for 1 μm thick analyses. The sensitivity of metasensor by tuning the thickness of the L-carnitine at 1.39 THz is given in supplementary materials of Section 6, which proves that our method can effectively retrieve the fingerprint signal even if the thickness of analyte is 10 μm. The pixel resonances provide linewidths narrower than the spectral feature size of the D-carnitine and L-carnitine absorption bands near 1.39 and 1.72 THz. This advantage allows us to read out the chiral substance absorption signature at broadband discrete frequency.

In experiment, D-carnitine and L-carnitine samples were purchased from Aladdin Corporation. To assess the trace detection, a total of 55 mg of sample powder and 1 mL of water was put into the test tube. Then 1 μL solution was ingested and transferred to the surface by using a pipette. The droplet was distributed on the surface in a circular shape with a diameter of 3 mm [39]. Firstly, the test results of D-carnitine and

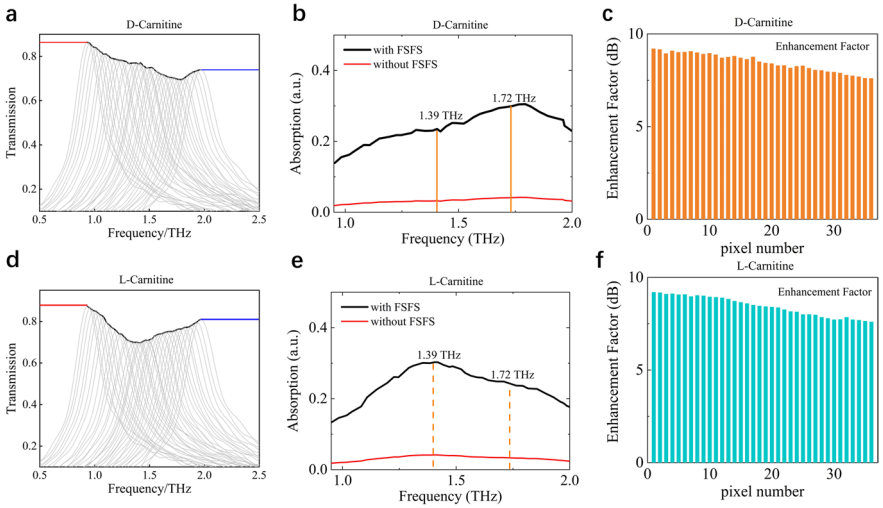

Fig. 6 Measured transmission spectra of coating 10 μm thick (**a**) D-carnitine and (**d**) L-carnitine on the FSFS. Envelope absorbance signals of (**b**) D-carnitine and (**e**) L-carnitine. Broadband sensing enhancement factor with respect to pixel number for (**c**) D-carnitine and (**f**) L-carnitine

L-carnitine between the tablet pressing method and the thin film detection on the glass surface are given in supplementary materials of Section 7. The absorption peaks obtained in the tablet pressing test are strong, while in the thin film test, it can be observed that the absorbance is relatively weak and the absorption peaks can hardly be observed. Then, the multiplexed transmission spectra and their peak envelope of coating the trace D-carnitine and L-carnitine with thickness of 10 μm on the metasurface are plotted in Fig. 6a and d, respectively. Such two envelopes clearly reflect the fingerprint features of D-carnitine and L-carnitine. The absorption characteristics of D-carnitine and L-carnitine are revealed by calculating the absorbance signal, as shown in Fig. 6b and e, which is in good agreement with the absorbance characteristic signal (red line) without the FSFS. The enhancement factor can be expressed as:

$$F = 10\lg\left(\frac{A(\mathrm{n})}{A_{Ref}(n)}\right) \tag{3}$$

where A(n) and A_{Ref}(n) refer to the absorption of trace analyte on FSFS and unpatterned surface, respectively. n is defined as pixel number. The broadband enhancement factors of FSFS for trace D-carnitine and L-carnitine detection are plotted in Fig. 6c and f, respectively. The average enhancement factors for D-carnitine and L-carnitine are about 8.3 dB (6.8 times) and 8.65 dB (7.3 times) in the band of 0.95 THz—2.0 THz, respectively. The retrieved absorbance envelope amplifies the peak values to 24.1% and 30.3% (D-carnitine) and 30.9% and 25.2% (L-carnitine) at the frequencies of 1.39 THz and 1.72 THz, respectively. The enhancement factors also show relatively change with pixel number (frequency) because the wider pixel scanning has influences on the near-field distribution surrounding the chiral carnitine.

Table 1 Fingerprint detection of metasurface

Scheme	Multiplex	AIT (Enhancement factor)	Frequency range	Analyte	Enhancement factor	Comment
Dielectric metagrating [40]	Angle	/	Mid-IR	Isomer (hBN, cBN)	5.4 (Theory)	
Dielectric metagrating [30]	Angle/thickness	/	THz (0.9–1.6 THz)	Isomer (ε-HNIW, γ-HNIW)	79 (Theory)	Fluid and substrate hardly have same RI, making this composite multiplex unrealistic
Plasmonic metasurface [41]	Graphene-voltage/geometry	/	THz (1.2–2.7 THz)	glucose	5 (Theory)	
FSFS(This work)	Geometry	α-lactose (7)	THz (0.95–2 THz)	Chiral enantiomers (D-carnitine and L-carnitine)	7.3 (Experiment)	

Discussion and conclusion

Finally, we compared our work with several broadband enhanced fingerprint schemes for trace detection of isomers/chiral enantiomers, as listed in Table 1 [30, 40, 41]. The dielectric metagrating can achieve high enhancement factor with narrow spectral range. To achieve broad spectral range, dual degree of freedom reconfiguration spectral multiplexing mechanism should be proposed based on angle and thickness multiplex [30]. However, the fluid in microfluidic channel and substrate hardly have the same refractive index (RI) in experiment, making this composite multiplex unrealistic in practice. We proved that the FSFS platform can effectively boost the THz molecular fingerprint of trace chiral carnitines with enhancement factor of 8.65 dB (7.3 times) in 0.95 THz—2.0 THz. More importantly, it can also achieve AIT effect at nearby pixels group with maximum enhancement factor of 7. All the results show great potential in biochemical analysis and component identification. More recently, advanced frequency agility in the frequency domains can be achieved through integration of spatially reconfigurable microelectromechanical systems or phase change material into metamaterials [42–44]. By tune the resonance frequency actively, the broadband absorption fingerprint spectra can be enhanced and differentiated without the need for frequency scanning [41]. Such frequency-agile approach might provide control over frequency response of metamaterial for versatile miniaturized THz spectroscopy device [45].

In conclusion, FSFS was designed to enhance molecular fingerprint sensing both by AIT and by multiplexing technologies. In the previous design, dielectric metasurfaces are often used due to their ultrahigh Q factor. However, in THz range, such ultra-narrow linewidth of resonance is hardly detected due to limitation of frequency resolution of THz-TDS (typical 5–10 GHz). For analysis with narrow absorption line of analyzes, the resonance with broad linewidth can strongly interact with analyze to achieve clear AIT, which can exhibit the fingerprint spectral feature more clearly. For this reason, by

carefully designing the resonance linewidth of FSFS, we can achieve both robust AIT for narrow absorption line and enhanced fingerprint spectrum via multiplexing technology for broad absorption line. This work may have potential applications in boosting and identifying THz narrow and broad fingerprint spectra with low cost.

Abbreviations

FSFS	Frequency selective fingerprint sensor
AIT	Absorption induced transparency
THz	Terahertz
RI	Refractive index
THz-TDS	Terahertz time-domain spectroscopy

Supplementary Information

The online version contains supplementary material available at https://doi.org/10.1186/s43074-023-00108-1.

Additional file 1: Section 1. The equivalent resonant circuit of cross slot metasurface. **Section 2.** Polarization independent response of cross slot metasurface. **Section 3.** The experimental results for time domain and frequency domain spectroscopy. **Section 4.** The resonance frequencies deviation between simulation and experiment. **Section 5.** The analytical and fitting parameter analysis by the equivalent AIT model. **Section 6.** Effect of the thickness of chiral carnitine film on the performed of device. **Section 7.** Comparison the test results of D-carnitine and L-carnitine between the tablet pressing method and the thin film detection on the glass surface.

Acknowledgements

The authors acknowledge support from Dr. Abhishek Kumar from Nanyang Technological University for his fruitful discussions.

Authors' contributions

L.C. initiated and conceived the idea of frequency selective fingerprint sensor; J.M.L designed the samples, performed the theoretical simulations; J.M.L., S.Y.S., and L.C. designed the experiments, performed the measurement; Y.M.Z. and S.L.Z. conceived and supervised the study, and discussed and prepared the manuscript; J.M.L. and L.C. wrote the paper. All authors reviewed and approved the final manuscript.

Funding

Basic Science Center Project of the National Natural Science Foundation of China[Grant No. 61988102]; National Natural Science Foundation of China[Grant No. 62275157]; Shanghai Shuguang Program[Grant No. 18SG44]; 111 Project[Grant No. D18014].

Availability of data and materials

Data underlying the results presented in this paper are not publicly available at this time but may be obtained from the authors upon reasonable request.

Declarations

Ethics approval and consent to participate

Not applicable.

Consent for publication

Not applicable.

Competing interests

The authors declare that they have no competing interests.

Received: 5 July 2023 Revised: 2 September 2023 Accepted: 7 September 2023
Published online: 19 September 2023

References

1. Tseng Y-T, Chang H-Y, Harroun SG, Wu C-W, Wei S-C, Yuan Z, Chou H-L, Chen C-H, Huang C-C, Chang H-T. Self-assembled chiral gold Supramolecules with efficient laser absorption for Enantiospecific recognition of carnitine. Anal Chem. 2018;90:7283–91.
2. Ryu DH, Cho JY, Sadiq NB, Kim J-C, Lee B, Hamayun M, Lee TS, Kim HS, Park SH, Nho CW, Kim H-Y. Optimization of antioxidant, anti-diabetic, and anti-inflammatory activities and ganoderic acid content of differentially dried Ganoderma lucidum using response surface methodology. Food Chem. 2021;335:127645.

3. Griboff J, Carrizo JC, Bonansea RI, Valdés ME, Wunderlin DA, Amé MV. Multiantibiotic residues in commercial fish from Argentina. The presence of mixtures of antibiotics in edible fish, a challenge to health risk assessment. Food Chem. 2020;332:127380.
4. Begin JL, Alsaawy M, Bhardwaj R. Chiral discrimination by recollision enhanced femtosecond laser mass spectrometry. Sci Rep. 2020;10:14074.
5. Stolarska M, Bocian W, Sitkowski J, Naumczuk B, Bednarek E, Popławska M, Błażewicz A, Kozerski L. Cathinones - Routine NMR methodology for enantiomer discrimination and their absolute stereochemistry assignment, using R-BINOL. J Mol Struct. 2020;1219:128575.
6. Simmen B, Weymuth T, Reiher M. How many chiral centers can Raman optical activity spectroscopy distinguish in a molecule. J Phys Chem A. 2012;116(22):5410–9.
7. Wang Z, Peng Y, Shi C, Wang L, Chen X, Wu W, Wu X, Zhu Y, Zhang J, Cheng G, Zhuang S. Qualitative and quantitative recognition of chiral drugs based on terahertz spectroscopy. Analyst. 2021;146:3888.
8. Losman J-A, Looper RE, Koivunen P, Lee S, Schneider RK, McMahon C, Cowley GS, Root DE, Ebert BL, Kaelin WG. (R)-2-Hydroxyglutarate Is Sufficient to Promote Leukemogenesis and Its Effects Are Reversible. Science. 2013;339:1621.
9. Liu K, Brown MG, Saykally RJ. Terahertz laser vibration rotation tunneling spectroscopy and dipole moment of a cage form of the water hexamer. J Phys Chem A. 1997;101(48):8995–9010.
10. Markelz AG, Roitberg A, Heilweil EJ. Pulsed terahertz spectroscopy of DNA, bovine serum albumin and collagen between 0.1 and 2.0 THz. Chem Phys Lett. 2000;320:42–8.
11. Nguyen KL, Friščić T, Day GM, Gladden LF, Jones W. Terahertz time-domain spectroscopy and the quantitative monitoring of mechanochemical cocrystal formation. Nat Mater. 2007;6(3):206–9.
12. Fasman GD, Bodenheimer E, Lindblow C. Optical rotatory dispersion studies of Poly-L-tyrosine and copolymers of L-glutamic acid and L-tyrosine. Significance of the tyrosyl Cotton effects with respect to protein conformation. Biochemistry. 1964;3(11):1665–74.
13. Zhang Z, Zhong C, Fan F, Liu G, Chang S. Terahertz polarization and chirality sensing for amino acid solution based on chiral metasurface sensor. Sens Actuators, B Chem. 2021;330:129315.
14. Quesada-Moreno MM, Virgili A, Monteagudo E, Claramunt RM, Aviles-Moreno JR, Lopez-Gonzalez JJ, Alkorta I, Elguero J. A vibrational circular dichroism (VCD) methodology for the measurement of enantiomeric excess in chiral compounds in the solid phase and for the complementary use of NMR and VCD techniques in solution: The camphor case. Analyst. 2018;143:1406–16.
15. Xu J, Liao D, Gupta M, Zhu Y, Zhuang S, Singh R, Chen L. Terahertz microfluidic sensing with dual-torus toroidal Metasurfaces. Adv Optical Mater. 2021;9:2100024.
16. Gupta M, Singh R. Terahertz Sensing with Optimized Q/V_{eff} Metasurface Cavities. Adv Optical Mater. 2020;8:1902025.
17. Shih K, Pitchappa P, Manjappa M, Ho CP, Singh R, Lee C. Microfluidic metamaterial sensor: Selective trapping and remote sensing of microparticles. J Appl Phys. 2017;121:023102.
18. Tan TC, Srivastava YK, et al. Active Control of Nanodielectric-Induced THz Quasi-BIC in Flexible Metasurfaces: A Platform for Modulation and Sensing. Adv Mater. 2021;9:2100836.
19 Kumar A, et al. Topological sensor on a silicon chip. Appl Phys Lett. 2022;121:011101.
20. Manjappa M, Pitchappa P, Wang N, Lee C, Singh R. Active Control of Resonant Cloaking in a Terahertz MEMS Metamaterial. Adv Optical Mater. 2018;6:1800141.
21. Chen L, Liao D, Guo X, Zhao J, Zhu Y, Zhuang S. Terahertz time-domain spectroscopy and micro-cavity components for probing samples: a review. Front Inf Technol Electron Eng. 2019;20(5):591–607.
22. Lin S, Xinlong Xu, Fangrong Hu, Chen Z, Wang Y, Zhang L, Peng Z, Li D, Zeng L, Chen Y, Wang Z. Using antibody modified terahertz metamaterial biosensor to detect concentration of carcinoembryonic antigen. IEEE J Sel Top Quantum Electron. 2020;27(4):6900207.
23. Lin S, Wang Y, Peng Z, Chen Z, Fangrong Hu. Detection of cancer biomarkers CA125 and CA199 via terahertz metasurface immunosensor. Talanta. 2022;248:123628.
24. Zeng Q, Liu W, Lin S, Chen Z, Zeng L, Fangrong Hu. Aptamer HB5 modified terahertz metasurface biosensor used for specific detection of HER2. Sens Actuators, B Chem. 2022;355:131337.
25. Shen F, Qin J, Han Z. Planar antenna array as a highly sensitive terahertz sensor. Appl Opt. 2019;58:540–4.
26. Xie J, Zhu X, Zang X, Cheng Q, Chen L, Zhu Y. Metamaterial-enhanced terahertz vibrational spectroscopy for thin film detection. Optical Materials Express. 2018;8(1):128–35.
27. Tittl A, Leitis A, Liu M, Yesilkoy F, Choi D-Y, Neshev DN, Kivshar YS, Altug H. Imaging-based molecular barcoding with pixelated dielectric metasurfaces. Science. 2018;360:1105.
28 Leitis A, Tittl A, Liu M, Lee BH, Gu MB, Kovshar YS, Altug H. Angle-multiplexed all-dielectric metasurfaces for broadband molecular fingerprint retrieval. Sci Adv. 2019;5:eaaw2871.
29. Zhu J, Jiang S, Xie Y, Li F, Du L, Meng K, Zhu L, Zhou J. Enhancing terahertz molecular fingerprint detection by a dielectric metagrating. Opt Lett. 2020;45:2335.
30. Xie Y, Ma Y, Liu X, Khan SA, Chen W, Zhu L, Zhu J, Liu Q. Dual-degree of freedom multiplexed Metasensor based on quasi-BICs for boosting broadband trace isomer detection by THz Molecular Fingerprint. IEEE J Sel Top Quantum Electron. 2023;29(5):8600110.
31. Rodrigo SG, Garcia-Vidal FJ, Martin-Moreno L. Theory of absorption-induced transparency. Phys Rev B. 2013;88:155126.
32. Hutchison JA, O'Carroll DM, Schwartz T, Genet C, Ebbesen TW. Absorption-induced transparency. Angew Chem Int Ed. 2011;50(9):2085–9.
33. Chen L, Xu N, Singh L, Cui T, Singh R, Zhu Y, Zhang W. Defect-induced Fano resonances in corrugated plasmonic metamaterials. Adv Opt Mater. 2017;5(8):1600960.
34. Chen L, Wei Y, Zang X, Zhu Y, Zhuang S. Excitation of dark multipolar plasmonic resonances at terahertz frequencies. Sci Rep. 2016;6:22027.
35. Nolte DD, Lange AE, Richards PL. Far-infrared dichroic bandpass filters. Appl Opt. 1985;24(10):1541.
36. Lin Y, Yao H, Ju X, Chen Y, Zhong S, Wang X. Free-standing double-layer terahertz bandpass filters fabricated by femtosecond laser micro-machining. Opt Express. 2017;25:25125–34.

37. Sun P, Zou Y. Complex dielectric properties of anhydrous polycrystalline glucose in the terahertz region. Opt Quantum Electron. 2016;48:1–10.
38. Ng B, Hanham SM, Wu J, Fernandez-Domnguez AI, Klein N, Liew YF, Breese M, Hong M, Maier SA. Broadband Terahertz Sensing on Spoof Plasmon Surfaces. ACS Photonics. 2014;1:1059–67.
39. Hu S, Sun C, Wu X, Peng Y. Polarization-Independent Terahertz Surface Plasmon resonance biosensor for species identification of Panax and Paeonia. Photonics. 2023;10:250.
40. Xie Y, Liu X, Li F, Zhu J, Feng N. Ultra-wideband enhancement on mid-infrared fingerprint sensing for 2D materials and analytes of monolayers by a metagrating. Nanophotonics. 2020;9:2927–35.
41. Sun L, Xu L, Wang J, Jiao Y, Ma Z, Ma Z, Chang C, Yang X, Wang R. A pixelated frequency-agile metasurface for broadband terahertz molecular fingerprint sensing. Nanoscale. 2022;14:9681.
42. Pitchappa P, Kumar A, Liang H, Prakash S, Wang N, Bettiol AA, Venkatesan T, Lee C, Singh R, Metamaterials F-A. Adv Optical Mater. 2020;8:2000101.
43. Xiaofei Z, Bingshuang Y, Lin C, Jingya X, Xuguang G, Alexei VB, Alexander PS, Songlin Z. Metasurfaces for manipulating terahertz waves. Light Adv Manuf. 2021;2:10.
44. Zhu Y, Zang X, Chi H, Zhou Y, Zhu Y, Zhuang S. Metasurfaces designed by a bidirectional deep neural network and iterative algorithm for generating quantitative field distributions. Light Adv Manuf. 2023;4:9.
45. Peng Y, Huang J, Luo J, Yang Z, Liping Wang XuWu, Zang X, Chen Yu, Min Gu, Qing Hu, Zhang X, Zhu Y, Zhuang S. Three-step one-way model in terahertz biomedical detection. PhotoniX. 2021;2:12.

Publisher's Note